Protein Science (1997), 6:2107–2119. Cambridge University Press. Printed in the USA.

Phosphorylation on histidine is accompanied by localized structural changes in the phosphocarrier protein, HPr from *Bacillus subtilis*

BRYAN E. JONES, PONNI RAJAGOPAL, AND RACHEL E. KLEVIT

University of Washington, Department of Biochemistry and Biomolecular Structure Center, Seattle, Washington 98195-7742

(RECEIVED March 31, 1997; ACCEPTED May 28, 1997)

Abstract

The histidine-containing protein (HPr) of bacterial phosphoenolpyruvate:sugar phosphotransferase system (PTS) serves a central role in a series of phosphotransfer reactions used for the translocation of sugars across cell membranes. These studies report the high-definition solution structures of both the unphosphorylated and histidine phosphorylated (P-His) forms of HPr from *Bacillus subtilis*. Consistent with previous NMR studies, local conformational adjustments occur upon phosphorylation of His 15, which positions the phosphate group to serve as a hydrogen bond acceptor for the amide protons of Ala 16 and Arg 17 and to interact favorably with the α-helix macrodipole. However, the positively charged side chain of the highly conserved Arg 17 does not appear to interact directly with phospho-His 15, suggesting that Arg 17 plays a role in the recognition of other PTS enzymes or in phosphotransfer reactions directly. Unlike the results reported for *Escherichia coli* P-His HPr (Van Nuland NA, Boelens R, Scheek RM, Robillard GT, 1995, *J Mol Biol 246*:180–193), our data indicate that phosphorylation of His 15 is not accompanied by adoption of unfavorable backbone conformations for active site residues in *B. subtilis* P-Ser HPr.

Keywords: histidine phosphorylation; HPr, NMR, solution structure

Protein phosphorylation is a key step in both the function and regulation of many cellular processes. Phosphorylation at hydroxyl-containing residues (e.g., Tyr, Ser, and Thr) has been the subject of intense investigation due to its nearly universal role in the regulation of enzymatic activities. More recently, there have been an increasing number of reports describing the presence and function of histidine kinases and phosphatases (for reviews, see Hughes, 1994; Swanson et al., 1994; Matthews, 1995). The bacterial phosphoenolpyruvate:sugar phosphotransferase system provides an opportunity to study the structural effects histidine phosphorylation.

Scheme 1

$$\text{EI} + \text{phosphoenolpyruvate} \leftrightarrow \text{P-EI} + \text{pyruvate}$$
$$\text{P-Enzyme I} + \text{HPr} \leftrightarrow \text{P-His HPr} + \text{Enzyme I}$$
$$\text{P-His HPr} + \text{EIIA}^{\text{sugar}} \leftrightarrow \text{P-EIIA}^{\text{sugar}} + \text{HPr}$$
$$\text{P-EIIA}^{\text{sugar}} + \text{EIIB}^{\text{sugar}} \leftrightarrow \text{P-EIIB}^{\text{sugar}} + \text{EIIA}^{\text{sugar}}$$
$$\text{P-EIIB}^{\text{sugar}} + \text{sugar}_{\text{out}} \leftrightarrow \text{P-sugar}_{\text{in}} + \text{EIIB}^{\text{sugar}}.$$

The histidine-containing protein serves a central role in the translocation of sugars in bacteria via the PTS (Scheme 1; Postma et al., 1993; Herzberg & Klevit, 1994), which involves a number of phosphoprotein intermediates. Structures of the unphosphorylated forms of Enzyme I (EI), HPr, and Enzyme IIA (EIIA) have been determined by NMR (Wittekind et al., 1992; Kalbitzer & Hengstenberg, 1993; Van Nuland et al., 1994) and X-ray crystallography (Worthylake et al., 1991; Jia et al., 1993; Liao & Herzberg, 1994; Liao et al., 1996).

The unstable nature of the nitrogen–phosphorous bond in aqueous solution has, to this point, precluded structure determination of any histidine phosphorylated protein by X-ray crystallography. As first demonstrated by Wittekind and Klevit (1991), solution state studies can make use of in situ regeneration systems that allow

Reprint requests to: Rachel E. Klevit; University of Washington, Department of Biochemistry and Biomolecular Structure Center, Box 357742, Seattle, Washington 98195-7742; e-mail: klevit@u.washington.edu.

Abbreviations: HPr, histidine-containing protein from *Bacillus subtilis*; HMQC, heteronuclear multiple quantum coherence; HMQC-*J*, J-modulated heteronuclear multiple quantum coherence; HSQC, heteronuclear single quantum coherence; NOESY, NOE spectroscopy; P.E. COSY, primitive exclusive correlation spectroscopy; PEP, phosphoenolpyruvate; PTS, phosphoenolpyruvate: sugar phosphotransferase system; P-His HPr, HPr phosphorylated at His 15; ROESY, rotating frame Overhaüser effect spectroscopy; RMSD, RMS deviation; TOCSY, total correlation spectroscopy.

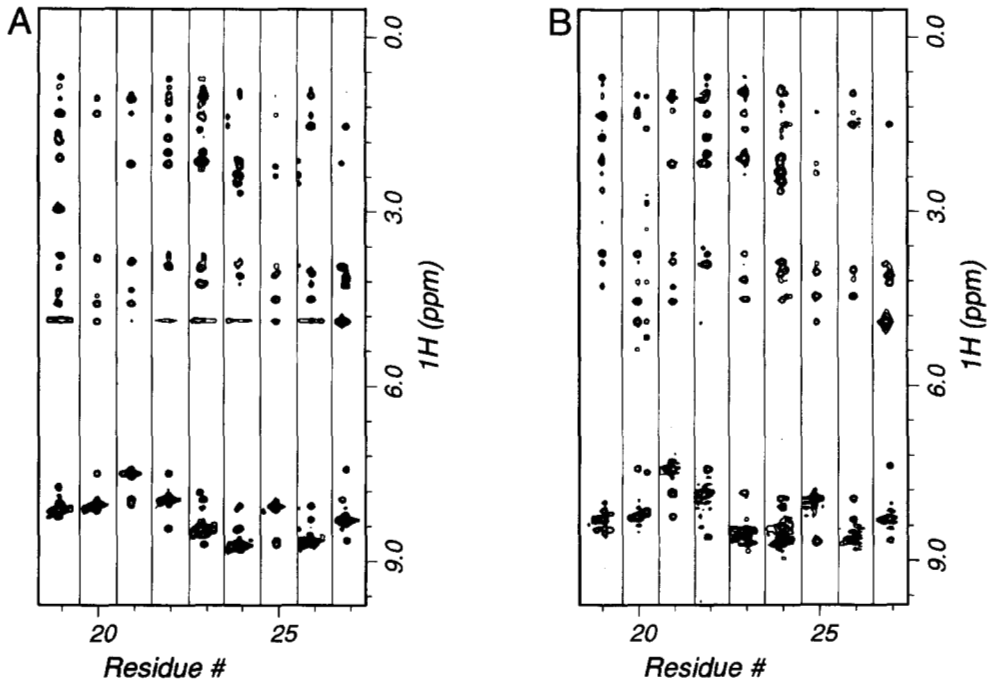

Fig. 1. Sections of strip plots taken from the ^{1}H-^{15}N-NOESY-HSQC experiments for native HPr (**A**) and P-His HPr (**B**). The spectrum of native HPr was recorded at pH 6.9, and 30 °C, and for P-His HPr, at pH 7.4 and 22 °C.

extended NMR experiments on the histidine phosphorylated forms of these proteins. NMR studies of the P-His forms of *Escherichia coli* EIIA (Pelton et al., 1992) and *Bacillus subtilis* HPr (Rajagopal et al., 1994) have provided insight on structural changes that occur near the site of phosphorylation. In addition, a solution structure of P-His HPr from *E. coli* determined using NMR data and restrained molecular dynamics has been reported (Van Nuland et al., 1995).

The results of previous NMR studies on the P-His form of *B. subtilis* HPr suggested that changes in the structure were localized to the region near His 15 (Rajagopal et al., 1994). However, a rigorous structure determination was not performed to confirm this supposition. Additionally, the low definition of the previous solution structure of *B. subtilis* HPr did not allow a detailed understanding of the effects of phosphorylation on the structure of HPr. In order to describe the structural changes that occur upon histidine phosphorylation in as much detail as possible, we have refined the previously determined solution structure of *B. subtilis* HPr, and determined the 3D solution structure of P-His HPr.

Results

Refinement of the native structure

The solution structure of *B. subtilis* HPr published previously was calculated on the basis of distance restraints obtained from 2D homonuclear and heteronuclear NOESY experiments (Wittekind et al., 1992). This model was of sufficient definition to understand general aspects of the structure of HPr, but lacked the definition required for discerning details in structural changes that occur upon phosphorylation. Therefore, the structure of the native protein was refined with the use of NOE constraints obtained from two 3D NOESY experiments that supplemented or replaced constraints determined previously (Wittekind et al., 1992).

Complete assignment of the side-chain ^{13}C and ^{1}H resonances was accomplished with the use of ^{1}H assignments published previously (Wittekind et al., 1990, 1992), and a combination of ^{1}H-^{13}C-HMQC and ^{1}H-^{13}C-HCCH-TOCSY experiments. This approach yielded unambiguous assignments for nearly all side-chain ^{13}C and ^{1}H resonances and confirmed the majority of ^{1}H assignments published previously (Wittekind et al., 1990); the only corrections necessary were the reassignment of the side-chain ^{1}H resonances of Arg 17, Pro 18, and Ile 55.

NOE constraints used to refine the native structure were obtained from two 3D NOESY experiments. ^{1}H-^{15}N-NOESY-HSQC (Sklenar et al., 1993), in which solvent suppression was achieved with pulsed field gradients instead of presaturation, was used to replace previously determined NOE constraints involving exchangeable amide protons, whose intensities may have been affected by solvent presaturation. A selected region of this spectrum is shown in Figure 1. A total of 634 unambiguous NOEs were identified in this spectrum. A 3D ^{1}H-^{13}C-NOESY-HMQC was used to obtain NOE connectivities between ^{13}C bound protons. Although only 141 *new* NOEs were identified in the 3D ^{1}H-^{13}C-NOESY, it served to confirm NOEs used in the original set of distance constraints, and provided additional constraints that were obscured by overlapped crosspeaks in the 3D ^{1}H-^{15}N-NOESY.

In total, 1,017 experimental distance constraints, including 74 hydrogen bond constraints determined previously and 125 dihedral angle constraints determined previously (Wittekind et al., 1992), were used in the structure calculation. The distribution of the distance constraints is shown in Figure 2. Except for residues Ser 12 and Gly13, and to a lesser extent, Gly 49–Ser 52 and Lys 82–Gly 85, there are a large number of constraints per residue. The new set of distance constraints contains 257 additional constraints compared to the data set used to calculate the previous solution structure. The majority of new constraints (~80%) are interresidue

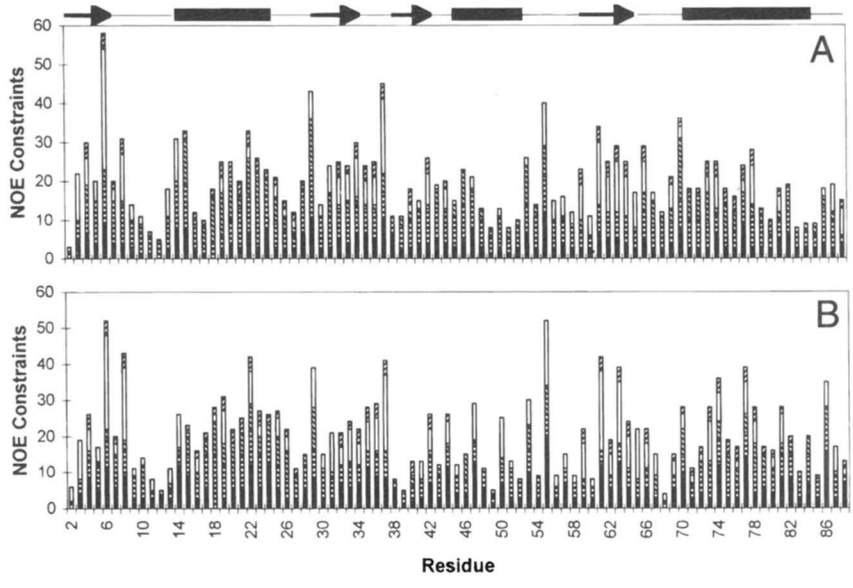

Fig. 2. Distribution of NOE constraints for the native (**A**) and P-His HPr (**B**) structure calculations. Constraints are grouped into intraresidue (i, i; ■), sequential (i, $i + 1$; ⊟), medium-range (i, $i + 2$–4; ▨), long-range (i, $i + >4$; □), and hydrogen bonds (▨). All NOE constraints, except intraresidue constraints, are counted twice in this figure. Secondary structural elements are shown above A.

constraints (83 $i \rightarrow i + 1$, 61 $i \rightarrow i + 2$–4, and 61 $i \rightarrow i + >4$), which are distributed evenly throughout the protein. Importantly, the new constraints provide a substantial number of long-range contacts between various segments of the protein that are necessary for the accurate placement of secondary structural elements relative to one another.

A set of 40 structures was calculated with X-PLOR (v. 3.1; Brünger, 1993) using a hybrid distance geometry/simulated annealing protocol (Nilges et al., 1988). Of the set of 40 structures, 30 had no NOE constraint violations greater than 0.3 Å and no dihedral angle constraint violations greater than 3°. The top 25 structures, based on their total energy calculated in X-PLOR, were selected for detailed analysis. The good superposition of these 25 structures shows that the experimental constraints define the 3D structure of HPr well (Fig. 3A). Secondary structure elements, as determined with the program KSDSSP [supplied with MidasPlus; (Kabsch & Sander, 1983; Ferrin et al., 1988)], are indicated on the ribbon representation of the minimized average structure (Fig. 3B).

The agreement of the set of structures with the experimental data is shown in Table 1. The small deviations from ideal covalent geometry and large, negative Lennard–Jones energy indicate that the calculated structures have good geometry (Table 1). Ramachandran plots of both the set of structures and of the minimized average structure indicate that the backbone geometry is also good; 100% of the residues are in allowed regions and 87% lie in most-favored regions for the minimized, average structure (data not shown).

The high definition of the refined structure is also exhibited in plots of the average pairwise ⟨RMSD⟩ for both backbone and side-chain atoms (Fig. 4A,B). The average values of 0.7 Å and 1.2 Å for the backbone and side-chain atoms, respectively, over the entire molecule, are a significant improvement over the previous solution structure. Regions that exhibit the largest deviation in the backbone position correspond to those that are deficient in distance constraints (e.g., the loop containing Ser 12, and residues near Val 50). However, the residues forming Helix-B (Ser 46–Leu 53) are better defined in this set of structures compared to the set of structures published previously; the ⟨RMSD⟩ values are ~1–1.5 Å for the backbone atoms of Helix-B in this set of structures, compared to ~2 Å in the structure published previously (Wittekind et al., 1992).

A comparison of individual dihedral angles in the set of structures, independent of relative atomic positions in the set, is afforded by the order parameter, $\langle S^2 \rangle$ (Hyberts et al., 1992). Values ranging from unity (where all of the compared structures have identical values for a particular dihedral angle) to 0 (where the value of the particular dihedral angle is distributed randomly within the set of structures) can be observed. The order parameter for the backbone dihedrals ϕ and ψ, and for the side-chain dihedral χ_1 are shown in Figure 4C, D, and E, respectively. Order parameters much less than 1 are only observed for backbone dihedrals of residues in loops, indicating that the backbone conformation is well defined by the experimental constraints. Except for a few residues, the order parameters for the χ_1 indicate that most side chains are well defined by the experimental constraints; the exceptions are all solvent-exposed residues that have few NOE contacts with the rest of the protein.

Determination of the histidine-phosphorylated structure

The strategy undertaken for the determination of the structure of P-His HPr was similar to that described above. The instability of the P-His side chain in solution requires the use of an in situ regeneration system (Wittekind & Klevit, 1991; Rajagopal et al., 1994). In this system, an excess of PEP and a catalytic amount of EI is added to the sample. Under these conditions, HPr can be kept phosphorylated for more than 3 days, sufficient to acquire 3D NMR experiments.

Complete assignments of all ^{1}H and aliphatic ^{13}C resonances were accomplished with a combination of ^{1}H-^{15}N-edited HMQC-TOCSY and ^{1}H-^{13}C-HCCH-TOCSY experiments. NOE constraints for P-His HPr were determined in an analogous fashion to the native protein. The elevated pH required to maintain histidine phos-

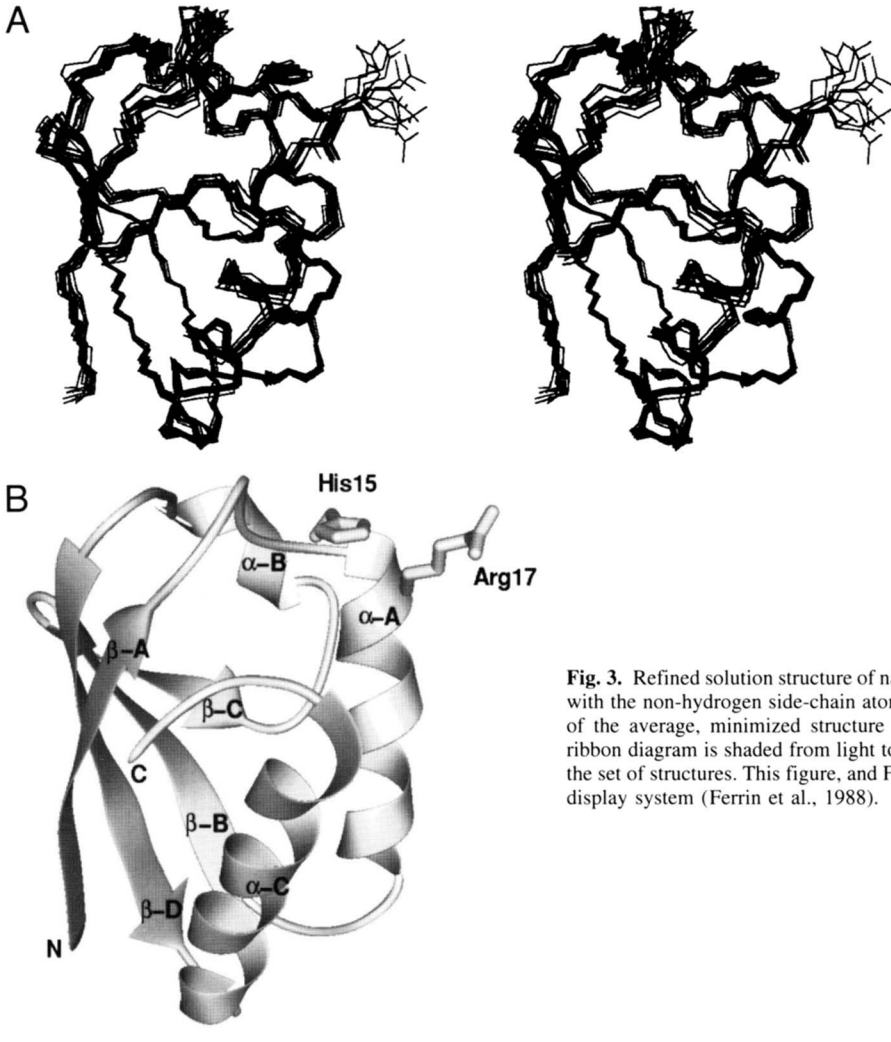

Fig. 3. Refined solution structure of native HPr.[1] **A:** Superposition of the top 25 structures with the non-hydrogen side-chain atoms of His 15 and Arg 17. **B:** Ribbon representation of the average, minimized structure with secondary structure elements indicated. The ribbon diagram is shaded from light to dark gray according to the RMSD of the atoms in the set of structures. This figure, and Figures 5 and 7, were generated using the MidasPlus display system (Ferrin et al., 1988).

phorylation (pH 7.4, compared to pH 6.9 for the native protein) required the use of a sensitivity-enhanced ^{1}H-^{15}N-NOESY-HSQC, which utilizes pulsed-field gradients for coherence selection and employs a water "flip-back" pulse for minimization of cross saturation due to solvent exchange (Zhang et al., 1994); representative data from this experiment are shown in Figure 1. Additional experiments included a ^{1}H-^{13}C-HSQC-NOESY (Majumdar & Zuiderweg, 1993) for determining NOE connectivities between aliphatic ^{13}C bound protons, and a 2D homonuclear NOESY (in $^{2}H_2O$) to obtain NOE constraints for the aromatic and P-His side chains.

A total of 1,136 distance constraints were used; 618 were obtained from the ^{1}H-^{15}N-NOESY, 386 were obtained from the ^{1}H-^{13}C-NOESY, 58 were obtained from the 2D homonuclear NOESY, and the set of 75 hydrogen bond constraints used for the native structure determination were used. The distribution of NOE constraints are shown in Figure 2B. As with the native protein, only the loop regions are lacking in NOE constraints.

With one exception, matched HMQC-*J*, HNHB, and P.E. COSY experiments (Rajagopal et al., 1994) indicated that no measurable changes in coupling constants were detected in P-His HPr. Therefore, the dihedral angle constraints used for the native protein were also used in the calculation of the P-His HPr structure. The only exception was that Arg 17 appears to be conformationally averaged in the native protein, but appears to adopt a single χ_1 rotamer in P-His HPr (Rajagopal et al., 1994). Spectral overlap in the P.E. COSY prevented stereospecific assignments of the H_βs of Arg 17, therefore no χ_1 constraint was used for the calculation.

Structure calculations for P-His HPr included a phosphoryl group (PO_3^{2-}) attached to the N_δ of His 15; the imidazole ring was also protonated at the N_ϵ, consistent with measurements of the tautomeric state of P-His HPr at pH 7.4 (Rajagopal et al., 1994). The covalent geometry was based on small molecule crystal structures of phosphoramidates, and was essentially identical to the energy-minimized geometry by van Nuland et al. (1996). Forty structures were calculated in X-PLOR as described above; 35 structures had no NOE violations greater than 0.3 Å, and no dihedral violations greater than 0.3°. The superposition of the top 25 structures and a ribbon representation indicating secondary structure elements are shown in Figure 5. The structure of P-His HPr is well defined, as evidenced by plots of atomic ⟨RMSD⟩s (Fig. 6A,B) and angle order parameters (Fig. 6C,D,E). Although the ⟨RMSD⟩ values are

[1]Atomic coordinates for both native (2HID) and P-His HPr (1JEM) structures have been submitted to the Protein Data Bank. All structure coordinates, NMR assignments, and X-PLOR constraint files can be obtained via the World Wide Web at http://mozart.bmsc.washington.edu/~klevit/hpr.html.

Table 1. *Structure calculation statistics and RMS differences*

RMSDs from experimental constraints	Native HPr[a]	P-His HPr
All NOE constraints (1035, 1136)[b] (Å)	0.0093 ± 0.0015	0.0130 ± 0.0019
Intraresidue NOE constraints (338, 443) (Å)	0.0062 ± 0.0023	0.0128 ± 0.0011
Sequential NOE constraints ($i \rightarrow i + 1$; 291, 242) (Å)	0.0121 ± 0.0028	0.0113 ± 0.0011
Medium-range NOE constraints ($i \rightarrow i + 2$–4; 178, 167) (Å)	0.0112 ± 0.0021	0.0201 ± 0.0105
Long-range NOE constraints ($i \rightarrow i + >4$; 164, 210) (Å)	0.0044 ± 0.0012	0.0089 ± 0.0011
H-bond NOE constraints (74, 74) (Å)	0.0084 ± 0.0013	0.0115 ± 0.0020
Experimental dihedral restraints (126, 126) (°)	0.099 ± 0.044	0.139 ± 0.058
Deviations from idealized geometry[c]		
Bonds (Å)	0.0025 ± 0.0001	0.0027 ± 0.0001
Angles (°)	0.378 ± 0.009	0.425 ± 0.008
Impropers (°)	0.260 ± 0.007	0.315 ± 0.009
Average energies		
E_{NOE} (kcal mol^{-1})[d]	0.089 ± 0.078	0.169 ± 0.160
E_{cdih} (kcal mol^{-1})[d]	6.43 ± 0.36	9.26 ± 0.58
E_{repel} (kcal mol^{-1})[e]	4.43 ± 1.49	9.78 ± 2.84
$E_{L\text{-}J}$ (kcal mol^{-1})[f]	−253.6 ± 46.3	−208.1 ± 16.9
Average pairwise atomic RMS differences (Å)[g]		
Backbone atoms	0.69 ± 0.14	0.55 ± 0.08
All non-hydrogen atoms	1.17 ± 0.19	1.06 ± 0.09

[a]Values represent the averages over the set of the top 25 structures calculated. Error limits indicate the standard deviation.

[b]Numbers in parentheses indicate the total number of constraints for native and P-His HPr structure determinations, respectively. Total number of NOE constraints includes hydrogen bond constraints.

[c]Force constant values for bond, angle, and improper torsions were set to 100 kcal mol^{-1} Å^{-2}, 500 kcal mol^{-1} rad^{-2}, and 500 kcal mol^{-1} rad^{-2}, respectively.

[d]Square-well NOE and dihedral potentials were used, with force constants of 50 kcal mol^{-1} Å^{-2} and 200 kcal mol^{-1} rad^{-2}, respectively (Brünger, 1993).

[e]Value of the repulsion term was calculated with a force constant of 4 kcal mol^{-1} Å^{-4}, and the van der Waals radii set to 0.8 times the standard values.

[f]$E_{L\text{-}J}$ is the Lennard–Jones energy term calculated with the CHARMM empirical energy function. It is not included during the structure calculations, and is used only for comparison.

[g]RMS differences were obtained by calculating pairwise backbone and side-chain RMSDs for each individual structure to the remaining structures in the set. Average values and standard deviations are shown.

slightly lower for P-His HPr, the loop regions exhibit higher deviations compared to the native structure. The increased ⟨RMSD⟩ most likely is caused by a lack of NOEs (or decreased intensity, Fig. 2B) involving the amide protons in the loop regions due to the higher solution pH used for studying P-His HPr.

Comparison of native and P-His HPr

Results of a quantitative comparison of the sets of structures for native and P-His HPr are shown in Figure 7. Average pairwise RMSD values for the backbone and side-chain atoms reveal that, overall, the structures are very similar, as can be seen in the superposition of ribbon representations of the average structures (Fig. 8); the average RMSDs for the backbone and side-chain atoms for the whole molecule are 0.82 Å and 1.31 Å, respectively. The largest deviations in backbone conformations occur primarily in regions that are ill-defined in either one or both sets of structures (e.g., residues 12–14, 38–40, and 51–53). With a few exceptions, the ⟨RMSD⟩ values for the side-chain atoms mirror the results for the backbone atoms, the exceptions being residues that extend directly into solvent, and make little contact with the remainder of the protein. As expected from the positional differences, plots of the difference in the average ϕ, ψ, and χ_1 dihedral values are very similar except in ill-defined regions of the structures (Fig. 8). These data indicate that histidine phosphorylation does not affect the overall structure of HPr.

A close inspection of the region near His 15 (Fig. 8B) reveals the local structural changes that occur upon His 15 phosphorylation. The largest change is the repositioning of the His 15 side chain toward solvent and rotated slightly along the C_β-C_γ bond, accompanied by a change in the average χ_1 for His 15 from 38° (±5°) in the set of native structures to 65° (±3°) in the set of P-His HPr structures. The order parameters for the χ_1 dihedral for both structures are near 1 ($\langle S^2 \rangle$ is 0.9956 for native and 0.9986 for P-His HPr), indicating that the conformation of His 15 is well determined, and that this structural difference, although small, is significant. The disposition of the His 15 side chain results in the placement of the phosphate group over the amide protons of Ala 16 and Arg 17. As a result of the repositioning of His 15, there are significant differences in the backbone dihedral angles of Ile 14 and His 15; the average value of ψ for Ile 14 changes from 128° (±10°) to 79° (±7°), and the average value of ϕ for His 15 changes from −132° (±5°) to −103° (±6°). However, these changes still result in backbone dihedral angles that are within allowed regions of the Ramachandran plot.

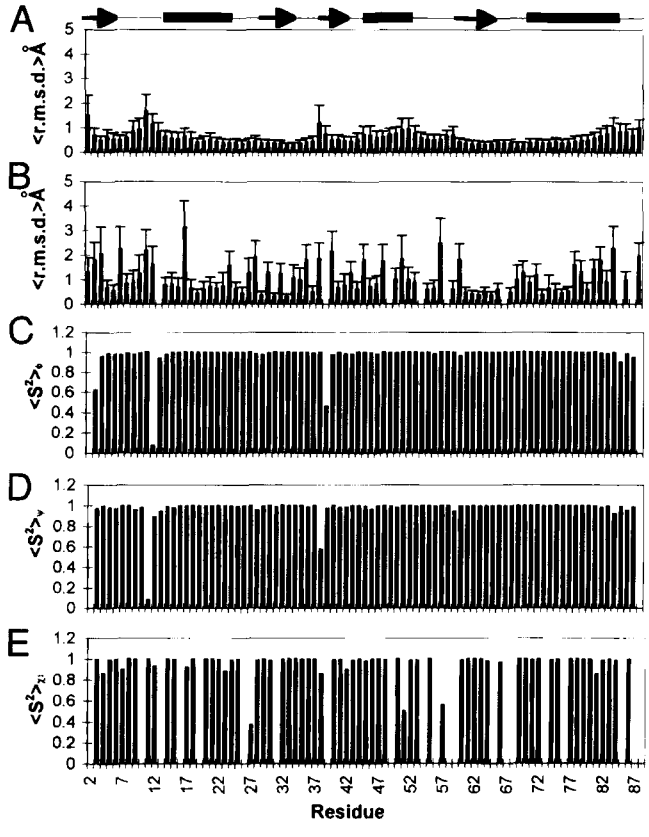

Fig. 4. Quantitative comparison of the set of native HPr structures. Average pairwise RMSDs for the backbone (**A**) and side-chain (**B**) non-hydrogen atoms are shown; error limits indicate the standard deviation. Angular order parameters $\langle S^2 \rangle$ (Hyberts et al., 1992) are shown for the ϕ (**C**), ψ (**D**), and χ_1 (**E**). Secondary structure is shown above A.

Amide hydrogen exchange rates

Previous experiments have shown that His phosphorylation results in significantly decreased amide hydrogen exchange rates for Ala 16 and Arg 17 (Rajagopal et al., 1994). Only a lower estimate of the exchange rate could be determined for these residues because the rate was too fast to be measured by persistence methods ($k \geq 0.1$ min^{-1}) and too slow to be measured by cross-saturation techniques [(Spera et al., 1991); $k \leq 1$ s^{-1}]. A more recently developed method (Grzesiek & Bax, 1993), which uses selective inversion of the water resonance, was used to measure exchange rates with solvent for both native and P-His HPr under identical conditions (pH 7.4, 22 °C).

The set of experiments necessary for determination of the solvent exchange rate included measurement of three relaxation parameters (^{15}N T_1, $^{15}N_z$-^1H_z longitudinal two-spin order, and ^1H_N $T_{1\rho}$ relaxation rates) as well as water-NOESY and water-ROESY experiments (which measure the NOE or ROE from water protons to each residue's amide proton). All experiments were collected on native and P-His HPr under identical solution conditions (those used for P-His HPr, 100 mM KPO_4, pH 7.4, at 22 °C). Only four residues that have exchange rates that fall within the measurable range of this experiment (~20 s^{-1} $\geq k \geq$ 0.2 s^{-1} at pH 7.4) exhibit a difference in their measured exchange rates; these results are summarized in Table 2.

The largest changes in hydrogen exchange rates occur for His 15, Ala 16, and Arg 17, whose rates decrease by factors of at least 10 for His 15 and Ala 16, and 6 for Arg 17. In general, the exchange rates calculated from the NOESY measurement (k_n) and the ROESY measurement (k_r) are equal within error for either native or P-His HPr for these residues, indicating that NOE buildup from water or nearby hydroxyl protons does not contribute significantly to the measured exchange rates (Grzesiek & Bax, 1993). For these residues, the two rates, k_n and k_r, are separate measurements of the solvent exchange rate, and their difference is indicative of the accuracy of the measurements. The exception, Ala 16 in P-His HPr, with a value of k_r less in magnitude and opposite in sign to k_n, indicates that NOE due to a water proton, or a nearby hydroxyl proton that exchanges with water, contributes significantly to the apparent exchange measured by k_n, implying that the true exchange rate with solvent for Ala 16 is actually slower than 0.5 s^{-1}(k_n). It is important to note that the measured rates should be considered as lower estimates of the true solvent exchange rates, because once the phosphohistidine is hydrolyzed, solvent exchange will occur at the measured rate of the native protein until His 15 is rephosphorylated. These results suggest that the amide protons of residues His 15–Arg 17 either experience a decrease in solvent accessibility or become protected by involvement in hydrogen bonds upon His 15 phosphorylation.

NMR relaxation measurements

Both the relative lack of definition in Helix-B in the structure of native HPr and the fast amide proton exchange rates for residues in Helix-B suggested that this region of HPr may be more mobile than the rest of the protein. Therefore, backbone amide ^{15}N relaxation experiments were performed to determine whether there is increased mobility in this region of the molecule. ^{15}N T_1, T_2, and heteronuclear NOE values for native HPr are essentially uniform for most of the molecule. The only exceptions are a few residues located near or within Helix-B, that show elevated T_2 relaxation rates (e.g., Lys 45 and Ile 47). These data indicate that the dynamic properties of the backbone of HPr are fairly uniform.

^{15}N T_1 and T_2 relaxation rates were also measured for P-His HPr and are shown in Figure 9. There are no significant differences in T_1 relaxation rates (within the standard error of the fits) and only a few differences in T_2 relaxation rates. The only residues to show significantly different T_2 relaxation rates (at the 85% confidence limit) are Ala 16 (7.11 ± 0.08 s^{-1} in the native HPr and 8.16 ± 0.24 s^{-1} in P-His HPr) and Arg 17 (7.84 ± 0.08 s^{-1} in native HPr and 8.49 ± 0.49 s^{-1} in P-His HPr). These data indicate that phosphorylation has little effect on the dynamic properties of HPr.

Discussion

Structural effects of His 15 phosphorylation

Previous NMR measurements indicated that the side chain of His 15 moves away from Ser 12 and toward the exterior of Helix-A (Rajagopal et al., 1994); His 15 resides in the N-1 position of this α-helix. The present structures confirm these initial hypotheses, and provide insight into how the phosphohistidine interacts with the protein. Its location at the N-terminus of Helix-A (Fig. 8) allows the phosphoryl group to interact favorably with the α-helix macrodipole (Hol et al., 1978; Hol, 1985). Interestingly, the his-

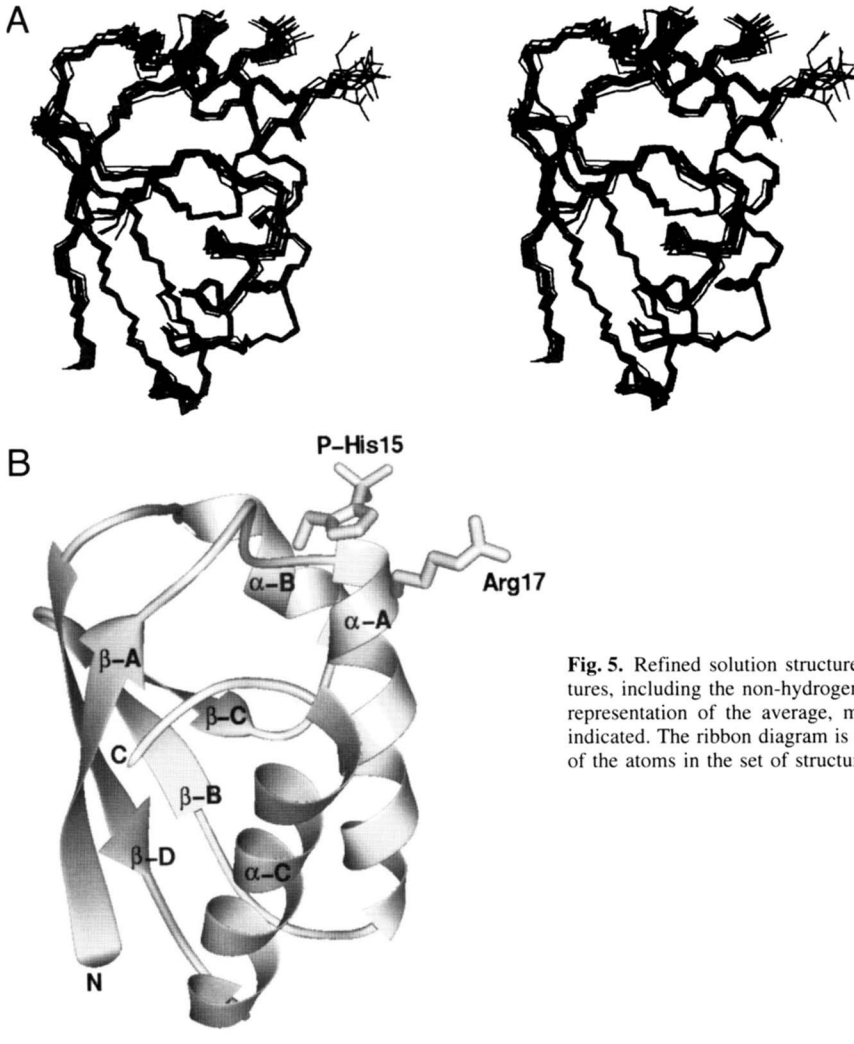

Fig. 5. Refined solution structure of P-His HPr.[1] **A:** Superposition of the top 25 structures, including the non-hydrogen side-chain atoms of P-His 15 and Arg 17. **B:** Ribbon representation of the average, minimized structure with secondary structure elements indicated. The ribbon diagram is shaded from light to dark gray according to the RMSD of the atoms in the set of structures.

tidines that become phosphorylated in EI (Liao et al., 1996) and EIIA (Worthylake et al., 1991) are also located structurally near the N-terminus of a helix, although in EIIA, the histidine is further away in sequence. Placement of phosphorylation sites near the N-terminus of α-helices has also been observed for proteins that are phosphorylated at other residues (Hurley et al., 1990; Zheng et al., 1993; Pullen et al., 1995), suggesting that this type of interaction may be a general motif in protein phosphorylation (Pullen et al., 1995).

The position of the phosphoryl group relative to the backbone atoms of Ala 16 and Arg 17 suggest that the phosphoryl oxygens may serve as hydrogen bond acceptors for the amide hydrogens of these two residues. The observed decrease in solvent exchange rates for these two residues supports this hypothesis. Close inspection of the local structure and orientation of the phosphate oxygens reveals that the geometry is not ideal for hydrogen bond formation, which may explain why the decreases in amide hydrogen exchange rates for Ala 16 and Arg 17 are fairly modest. Attempts to constrain the geometry of the phosphoryl group in order to allow for more favorable hydrogen bonding (by constraining the oxygen–nitrogen distances) invariably yielded ~10% higher overall calculated energies. Typically, only about 50% of the structures adopted a geometry that would provide more linear donor-to-acceptor angles, and appropriate distances for hydrogen bonds. Model building suggests that the placement of the phosphohistidine side chain is dominated by steric contacts with the backbone between His 15 and Ala 16, the methyl group of Ala 16, and the side-chain hydroxyl of Ser 12 (data not shown). Therefore, it is not surprising that ideal hydrogen bonding geometry is not observed.

It has also been suggested that the invariant Arg 17 may form a direct interaction with the P-His side chain (Liao & Herzberg, 1994). This hypothesis was thought to be supported by NMR measurements indicating that the χ_1 dihedral of Arg 17 becomes fixed upon phosphorylation (Rajagopal et al., 1994). HNHB spectra of native HPr exhibit no crosspeaks for Arg 17, indicative of either conformational averaging or a χ_1 of ~180°. A crosspeak is observed for Arg 17 in an HNHB spectrum of P-His HPr. A single crosspeak for one of the H_βs would be indicative of a χ_1 dihedral of either 60° or −60°, whereas a crosspeak for both H_βs would be indicative of a χ_1 of 180° or conformational averaging. However, the chemical shifts of the two H_βs are overlapped sufficiently that unambiguous interpretation of this result is difficult; this spectral overlap also prevents stereospecific assignment with a P.E. COSY experiment (Rajagopal et al., 1994). Of the three standard rotamers, a χ_1 of 180° is most consistent with the NOE data. The only NOE observed between the side chains of P-His 15 and Arg 17 is from the $H_{\epsilon 1}$ of His 15 to both the H_βs and H_δs of Arg 17. A χ_1 for Arg 17 of either 60° or −60° would place the H_γs of Arg 17 in close contact with the $H_{\epsilon 1}$ of His 15, and move the Arg 17 H_βs further away from the His side chain.

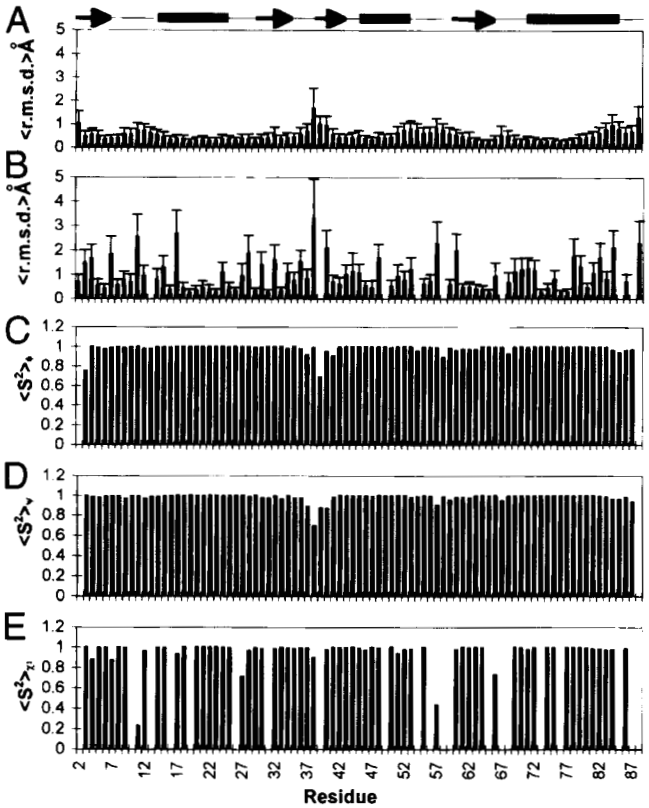

Fig. 6. Quantitative comparison of the set of P-His HPr structures. Average pairwise RMSDs for the backbone (**A**) and side-chain (**B**) non-hydrogen atoms are shown; error limits indicate the standard deviation. Angular order parameters $\langle S^2 \rangle$ (Hyberts et al., 1992) are shown for the ϕ (**C**), ψ (**D**), and χ_1 (**E**). Secondary structure is shown above A.

The effects of phosphorylation on the conformation of Arg 17 are small. The average χ_1 does not change significantly upon phosphorylation ($-120 \pm 25°$ in native HPr and $-123 \pm 21°$ in P-His HPr), although the order parameter for χ_1 increases from 0.919 in the native protein to 0.931 in P-His HPr. The increase in $\langle S^2 \rangle$ represents a decrease in the $\langle$RMSD$\rangle$ of the side-chain atoms (3.13 Å in the native protein and 2.68 Å in P-His HPr). However, it is likely that the apparent increase in the order of Arg 17 may be related to an increase in the number of potential steric interactions because of the presence of the phosphoryl group. As can be seen in the superposition of the sets of structures (Figs. 3A, 5A), the side chain of Arg 17 is disordered beyond the C_δ in both structures, suggesting that phosphorylation has little effect on the conformation of Arg 17.

Torsion angle strain

The structure of the histidine-phosphorylated form of *E. coli* HPr determined by constrained molecular dynamics suggested that phosphorylation results in unfavorable backbone dihedrals for His 15 and Ala 16 (Van Nuland et al., 1995, 1996). It was postulated that the torsion angle strain was released upon phosphotransfer to EIIA. The present structure of P-His HPr provides no indication of unfavorable backbone dihedral angles. Although phosphorylation does result in changes in the backbone conformation, the largest changes occur between Ile 14 and His 15, and the resultant dihedral angles are still within allowed regions of the Ramachandran plot (data not shown). These results indicate that, at least for *B. subtilis* HPr, histidine phosphorylation can be accommodated without unfavorable backbone conformations.

The conclusion that unfavorable backbone dihedral angles are formed upon phosphorylation was based on the observation of broadened amide ^{15}N resonances for His 15 and Thr 16 (Ala in *B. subtilis* HPr) in the P-His form compared to the unphosphorylated form. The observed line broadening was attributed to a change in the $^3J_{NH\alpha}$ for these residues. Conversely, it has been suggested that the line broadening may result from chemical exchange because the pK_a of His 15 in the phosphorylated state (pH 7.8; Rajagopal et al., 1994; Van Nuland et al., 1995) is close to the experimental pH (pH 7.4). Although the amide ^{15}N resonances for His 15, Ala 16, and Arg 17 are observed to be broadened in these studies as well (data not shown), matched (^1H, ^{15}N)-HMQC-*J* spectra (Bax et al., 1990) revealed no significant differences in any of the measured $^3J_{NH\alpha}$ coupling constants (Rajagopal et al., 1994). NMR relaxation experiments, which are sensitive to chemical exchange processes but not to changes in *J* coupling, indicate that the observed line broadening results from increased relaxation.

^{15}N T_2 measurements of HPr and P-His HPr are within error throughout the majority of the protein; the only residues to show significantly different T_2 relaxation rates are Ala 16 and Arg 17.

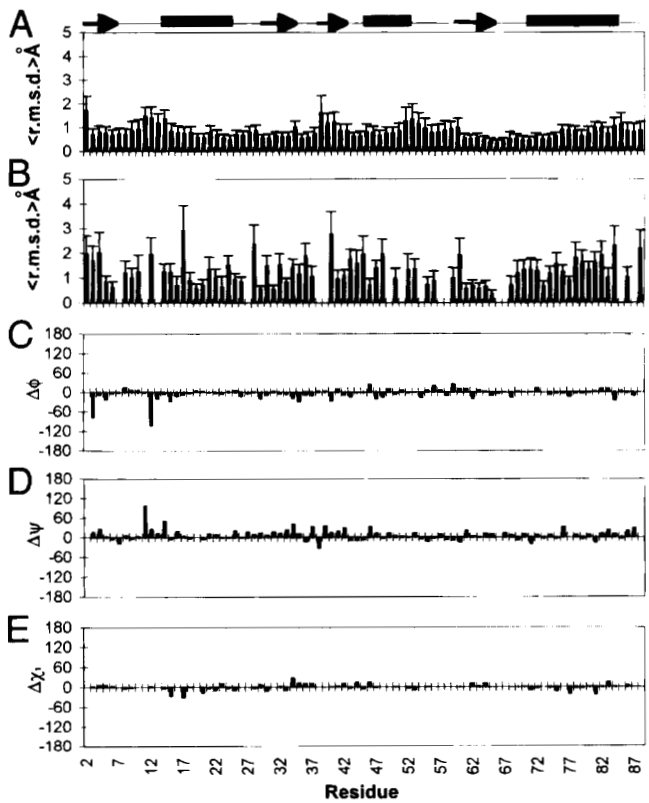

Fig. 7. Quantitative comparison of the sets of structures for native and P-His HPr. The average, pairwise RMSDs are shown for backbone (**A**) and side-chain (**B**) non-hydrogen atoms; error limits indicate the standard deviation. Differences in the average dihedral angles for ϕ (**C**), ψ (**D**), and χ_1 (**E**) are shown. A positive deviation indicates a clockwise rotation of the value in P-His HPr compared to the value in native HPr. Residues that have an order parameter for χ_1 less than 0.85 (which corresponds to a standard deviation of $\pm 30°$) are excluded in B and E. Secondary structure is shown above A.

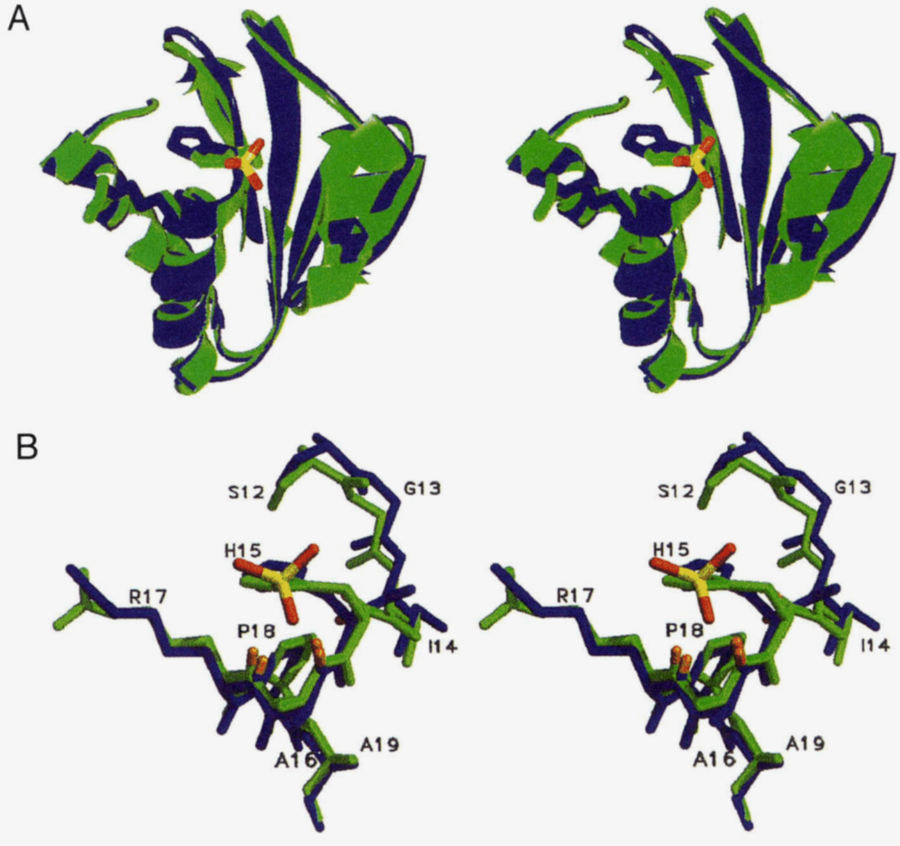

Fig. 8. Stereo views of the comparison of native and P-His HPr structures. **A:** Ribbon representations of native (blue) and P-His (green). **B:** Close-up view of the active-site region, with the amide protons of His 15, Ala 16, and Arg 17. This superposition was achieved by best fitting the backbone atoms of residues Ser 12–Pro 18 in MidasPlus (Ferrin et al., 1988).

Additionally, amide proton $T_{1\rho}$ measurements (data not shown) indicate that the amide proton of His 15, which points toward the P-His side chain, relaxes at nearly double the rate in P-His HPr ($52.9 \pm 6.8\ s^{-1}$) compared to the unphosphorylated form ($31.6 \pm 0.8\ s^{-1}$). Although this particular experiment is also sensitive to changes in solvent exchange rates (Grzesiek & Bax, 1993), the measured exchange rate for the amide hydrogen of His 15 decreases upon phosphorylation, implying that the measured relaxation rate is only a lower limit. Inspection of Figure 8 reveals that the amide nitrogens of Ala 16 and Arg 17, and the amide proton of His 15 are all very close to the imidazole ring, suggesting that chemical exchange of the P-His side chain, between the protonated and deprotonated forms, influences the relaxation of nearby atoms, and increases linewidths.

Table 2. *Comparison of solvent exchange rates for residues near His 15 in native and P-His HPr*

	Native HPr		P-His HPr	
Residue	k_n $(s^{-1})^a$	k_r $(s^{-1})^b$	k_n $(s^{-1})^a$	k_r $(s^{-1})^b$
Asp 11	23 ± 4	23 ± 6	9.0 ± 0.2	8.9 ± 0.5
His 15	1.0 ± 0.2	1.0 ± 0.2	0.2 ± 0.1	0.2 ± 0.1
Ala 16	6.2 ± 0.6	6.9 ± 0.9	0.5 ± 0.1	−0.2 ± 0.1
Arg 17	4.1 ± 0.3	5.1 ± 0.6	0.7 ± 0.1	0.7 ± 0.2

[a]Solvent exchange rate calculated based on the water-NOESY measurement at pH 7.4 and 22 °C; error limits are based upon propagation of standard errors in the relaxation measurements and the estimates of the RMS noise in the water-NOESY spectra.

[b]Solvent exchange rate calculated based on the water-ROESY measurement at pH 7.4 and 22 °C; error limits are based upon propagation of standard errors in the relaxation measurements and the estimates of the RMS noise in the water-ROESY spectra. Negative rates indicate that water-ROESY difference spectrum has a negative intensity, indicative of a significant contribution of NOE buildup to the calculated rate from a nearby water or rapidly exchanging hydroxyl proton.

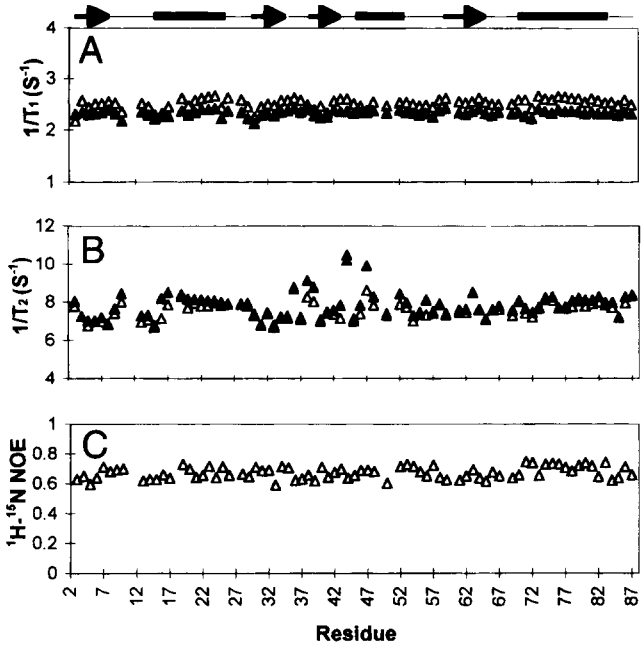

Fig. 9. ^{15}N relaxation parameters of native and P-His HPr. ^{15}N T_1 (**A**) and T_2 (**B**) relaxation rates are shown for both native (open symbols) and P-His (closed symbols). **C:** ^1H- ^{15}N heteronuclear NOE values for native HPr. Secondary structure is shown above A.

Implications for phosphotransfer

The structure of P-His HPr provides further insight into the phosphotransfer reaction between EIIA and HPr. A structural model for this reaction has been proposed based upon the X-ray structures of HPr and EIIA (Herzberg, 1992). The model proposes that the phosphotransfer reaction is triggered by a switch between two different salt bridges involving the guanidinium group of Arg 17. It is proposed that Arg 17 interacts with the phospho-His side chain prior to phosphotransfer. This supposition is based upon the side chain's interaction with a sulfate ion in the crystal structure; the sulfate is located near His 15, and is proposed to be a structural model for P-His HPr (Liao & Herzberg, 1994). During phosphotransfer, it is proposed that Arg 17 forms an intermolecular salt bridge with two invariant aspartate residues in EIIA (Asp 31 and Asp 87), and this would trigger the phosphotransfer reaction.

The present data indicate that the interaction between Arg 17 and phospho-His 15 is tentative at best. The observation that His 15 phosphorylation has little effect on the conformation of Arg 17 implies that the major role of Arg 17 may be to recognize the binding site for HPr on EIIA, and to align HPr in a proper orientation for phosphotransfer. Superposition of the minimized, average P-His HPr structure and the HPr structure in the model of the complex shows that the Arg 17 side-chain conformations are nearly identical. Interestingly, EI also has two highly conserved aspartates located structurally near the histidine that donates the phosphoryl group to HPr (Liao et al., 1996), suggesting that Arg 17 may play an analogous role in phosphotransfer to HPr from EI.

Materials and methods

Sample preparation

Expression and purification of *B. subtilis* HPr[2] was performed as described previously (Reizer et al., 1989; Wittekind et al., 1992). Isotopic labeling with either ^{15}N or ^{13}C was accomplished by using $^{15}NH_4Cl$ (99.5% isotopic enrichment; Isotec Inc.) or $^{13}C_6$-glucose (99.2% isotopic enrichment; Isotec Inc.). NMR samples were prepared by extensive dialysis against 5 mM potassium phosphate buffer, pH 6.9, containing 0.01 mM EDTA, followed by lyophilization. Lyophilized samples were dissolved in 500 μL of 90% H_2O/10% ^2H_2O containing 0.1 mM NaN_3. ^{15}N-labeled samples were typically 2–4 mM, ^{13}C-labeled sample was 2 mM, and doubly labeled ^{13}C, ^{15}N sample was 2 mM.

P-His HPr was produced in situ using a regeneration system comprised of excess phosphoenolpyruvate (PEP, 200 mM), 4 mM $MgCl_2$, 0.4 mM dithiothreitol, and a catalytic amount of EI (10 μg). NMR samples for phosphorylation experiments were prepared by extensive dialysis in 10 mM potassium phosphate buffer, pH 7.4, followed by lyophilization. Lyophilized samples were dissolved in the appropriate solvent, PEP, $MgCl_2$, and dithiothreitol were added, and the pH adjusted to 7.4 (uncorrected meter reading). The EI was added immediately prior to collecting NMR experiments. Using these conditions, HPr could be kept phosphorylated for more than 72 h. The extent of phosphorylation was checked before and after each experiment using a long-range HMQC-*J* experiment (Rajagopal et al., 1994) to monitor the chemical shifts of the His 15 $H_{\delta 2}$ and $H_{\epsilon 1}$ resonances. Because the chemical exchange between P-His and unphosphorylated HPr is slow on the NMR time scale, this experiment allows a direct measurement of the extent of phosphorylation (Rajagopal et al., 1994).

NMR spectroscopy

All NMR spectra (except the ^1H-^{13}C-HCCH-TOCSY and ^1H-^{13}C-NOESY-HMQC on the native protein) were recorded on a Brüker DMX-500 MHz spectrometer equipped with a ^1H, ^{15}N, ^{13}C triple resonance, triple axis gradient probe. All spectra of native HPr were collected at 30 °C and 22 °C for P-His HPr. The ^1H-^{13}C-HCCH-TOCSY (Bax et al., 1990) was recorded for native HPr on a Brüker AMX-600 MHz spectrometer (Brüker Instruments, Fremont, California). Spectral widths were 5,000 Hz (^1H), 5,000 Hz (^1H), and 10,000 Hz (^{13}C); the mixing time was 26 ms, and 16 scans per t_1 were recorded. The ^1H-^{13}C-HMQC (Bax et al., 1983) was acquired with spectral widths of 7,002 Hz (^1H) and 20,752 Hz (^{13}C), with 16 scans per t_1 increment. HNHB spectra (Archer et al., 1991), P.E. COSY, and ^{15}N-edited HMQC-TOCSY spectra were recorded as described previously (Wittekind et al., 1992; Rajagopal et al., 1994).

The ^1H-^{13}C-NOESY-HMQC for native HPr (Ikura et al., 1990) was recorded on a Brüker AMX 500-MHz spectrometer (Brüker Instruments). Spectral widths were 7,042 Hz (^1H), 7,042 Hz (^1H), and 20,833 Hz (^{13}C). The NOESY mixing time was 100 ms, and 16 scans were recorded per transient. The ^1H-^{15}N-NOESY-HSQC

[2]The "native" protein used in these studies contains a mutation from Met to Val at position 51, and is identical to the protein used in previous NMR studies in this laboratory. Previous biochemical studies have demonstrated that this mutation does not affect the function of HPr in vivo.

(Sklenar et al., 1993) was recorded as a matrix consisting of 64 complex points (^{15}N, t_1) × 256 complex points (^1H, t_2) × 512 (^1H, t_3) complex points. Spectral widths were 4,006 Hz (^1H) centered at the middle of the amide proton region of the spectra, 7,002 Hz (^1H), and 2,000 Hz (^{15}N) in t_3, t_2, and t_1, respectively. Solvent suppression was achieved with a WATERGATE sequence (Sklenar et al., 1993), using a 3-9-19 pulse train for selective excitation of the amide proton region. The NOESY mixing time was 100 ms, and this spectrum was recorded with 8 scans per transient.

The ^1H-^{13}C-HCCH-TOCSY (Kay et al., 1993) and ^1H-^{13}C-HSQC-NOESY (Majumdar & Zuiderweg, 1993) of P-His HPr were recorded on a doubly labeled sample dissolved in ^2H_2O. For the ^1H-^{13}C-HCCH-TOCSY, data were collected consisting 32 complex points (^{13}C, t_1) × 128 complex points (^1H, t_2) × 512 (^1H, t_3) complex points, with 8 scans per t_1 increment. Spectral widths were 5,000 Hz for both ^1H dimensions, and 2,641 Hz in the ^{13}C dimension. The ^1H-^{13}C-HSQC-NOESY was collected as 64 complex points (^{13}C, t_1) × 256 complex points (^1H, t_2) × 512 (^1H, t_3) complex points with 8 scans per fid. Spectral widths were 7,002.8 Hz for both ^1H dimensions, and 7,977 Hz in the ^{13}C dimension. The sensitivity-enhanced ^1H-^{15}N-NOESY-HSQC (Zhang et al., 1994), which employs gradient-based coherence selection and a "flip-back" pulse for water suppression, was collected as 256 complex points (^1H, t_1) × 64 complex points (^{15}N, t_2) × 512 (^1H, t_3) complex points, with 8 scans per fid. Spectral widths were 7,002.8 Hz for both ^1H dimensions, and 2,000 Hz in the ^{15}N dimension. Additionally, a 2D homonuclear NOESY was recorded with a 2-mM unlabeled P-His HPr sample dissolved in ^2H_2O. The spectrum was recorded as a 1,200 real (t_1) × 1,024 complex (t_2) matrix, with 64 scans per t_1 increment. Spectral widths were 7,002.8 Hz in both dimensions. The NOESY mixing time in all three experiments was 100 ms, and the TOCSY mixing time in the ^1H-^{13}C-HCCH-TOCSY was 26 ms.

Solvent exchange experiments

Water-NOESY and water-ROESY experiments used pulse sequences published previously (Grzesiek & Bax, 1993). The mixing times were 75 ms for the NOESY and 30 ms for the ROESY (at a spin-lock field strength of 8,000 kHz). Data with water magnetization aligned along the $+z$ and $-z$ axes were recorded in an interleaved fashion, and separated during processing into two separate matrices. Data were acquired with 56 scans, in two 128 × 512 complex matrices per experiment.

NMR relaxation measurements

^{15}N T_1, T_2, and heteronuclear NOE measurements were made using a pulse sequence published previously (Farrow et al., 1994), with one modification: the axes for gradient pulses were randomized for additional artifact suppression. ^{15}N T_1 measurements consisted of nine experiments with time intervals of 10, 90 (×2), 240, 400, 600 (×2), 900, and 1,200 ms (×2 indicates that the time point was repeated). ^{15}N T_2 measurements consisted of a set of nine spectra with time intervals of 14, 29, 43 (×2), 58, 86, 130 (×2), and 174 ms. Proton saturation in the heteronuclear NOE measurements was accomplished with 120° pulses every 5 ms for 3 s. $^{15}N_z$-^1H_z longitudinal two-spin order relaxation rates were measured with the pulse sequence described by Peng and Wagner (1994), modified to include WATERGATE solvent suppression (Sklenar et al., 1993). Nine experiments were recorded with time intervals of 10, 20, 30, 40, 60 (×2), 90, and 170 (×2) ms. Amide proton $T_{1\rho}$ measurements were accomplished using a modification of water-ROESY pulse sequence described by Grzesiek and Bax (1993). Eight spectra were recorded with a spin-lock field strength of 8,000 kHz, and with mixing times of 5, 10, 20 (×2), 40, 60 (×2), and 100 ms. Spectra were recorded as 256 × 512 complex matrices with 8 scans per t_1 point. Spectral widths in the ^{15}N and ^1H dimension were 2,000 and 7,002.8 Hz, respectively.

Data processing and analysis

NMR data were processed and analyzed with either FELIX 2.3 (Biosym Inc.) or NMRPIPES (Delaglio et al., 1995). All NOESY data and relaxation data were apodized with 90° phase shifted sine-bell squared functions prior to zero-filling and Fourier transformation. Unambiguously assigned NOE crosspeaks used for structure calculation were picked, and the volumes integrated using FELIX. Relaxation data and water exchange experiments were peak-picked and intensities measured using either FELIX or PIPP (Garrett et al., 1991). Intensities obtained in relaxation experiments were fit to a single exponential decay using NONLIN (Johnson & Frasier, 1985).

Experimental constraints

Unambiguously assigned NOEs were classified as being either strong, medium, weak, or very weak, and were assigned distance constraints of 1.85–2.85 Å, 1.85–3.85 Å, 1.85–4.50 Å, and 1.85–5.50 Å, respectively. In addition, amide hydrogens involved in hydrogen bonds were represented by two constraints, as described previously (Wittekind et al., 1992): the distance range for the amide proton to the carbonyl oxygen acceptor was 1.60–2.30 Å and the distance range for the amide nitrogen to the carbonyl oxygen was 2.50–3.30 Å. R^{-6} averaging was for degenerate protons of methyl and methylene groups in all structure calculations.

For refinement of the native structure, an initial set of distance constraints (Wittekind et al., 1992) served as a basis for the addition of new constraints determined from the two 3D NOESY experiments. First, nonredundant constraints identified in the ^1H-^{13}C-HMQC-NOESY were added. Then, all constraints involving exchangeable protons were replaced with bounds determined from the ^1H-^{15}N-NOESY-HSQC. The final NOE constraints file consisted of a total of 1,017 upper distance constraints: 332 intraresidue constraints, 301 i to $i + 1$ constraints, 50 i to $i + 2$ constraints, 63 i to $i + 3$ constraints, 28 i to $i + 4$ constraints, 162 long-range constraints, and 74 H-bond constraints.

For P-His HPr, a total of 1,137 distance constraints were used; 618 were obtained from the ^1H-^{15}N-NOESY-HSQC, 386 were obtained from the ^1H-^{13}C-HSQC-NOESY, 59 were obtained from the 2D homonuclear NOESY. Because the ^1H-^{13}C-HSQC-NOESY was recorded in ^2H_2O, the sets of NOE constraints from the two 3D experiments were mutually exclusive. In addition, the set hydrogen bond constraints used for the native structure determination was also used for the calculation of the P-His HPr structure.

Previously determined dihedral angle constraints, based on analysis of P.E. COSY spectra (Wittekind et al., 1992), were supplemented with additional χ_1 angle constraints determined from analysis of HNHB spectra in conjunction with intraresidue NOE information. The dihedral constraints used for structure calculation consisted of 71 ϕ and 55 χ_1 angle constraints. HMQC-J spectra and

P.E. COSY spectra indicated that His 15 phosphorylation resulted in no significant differences in backbone dihedrals, and that only the χ_1 of Arg 17 differed from the unphosphorylated form. Therefore, the same set of dihedral constraints were used in the calculation of both structures (Arg 17's χ_1 dihedral was not constrained in either structure).

Structure calculation

Solution structures were calculated using a hybrid distance geometry-simulated annealing protocol (Nilges et al., 1988) using the program X-PLOR (v. 3.1; Brünger, 1993). A family of 40 initial structures were generated and refined prior to selecting the best 25 for comparative analysis. Initial substructures (using only backbone heavy atoms and the C_β and C_γ) were embedded using the *dg_sub_embed* distance geometry procedure supplied with the software package. The coordinates of the remaining atoms were generated by template fitting and refined with simulated annealing using the supplied *dgsa* routine. The set of structures was further refined with the provided simulated annealing routine *refine*. The best 25 structures, based upon the overall calculated energy, were selected for detailed analysis. All structures in this set had no violations of NOE constraints greater than 0.3 Å, no dihedral angle constraint violations greater than 3°, and small deviations from ideal bond lengths and geometries (Table 1).

Pairwise RMSDs among the set of structures were calculated with X-PLOR. Average structures were calculated, and subjected to 500 steps of Powell minimization in X-PLOR to remove bad contacts and geometries resulting from the averaging of coordinates. The minimized average structures of HPr and P-His HPr had no experimental violations greater than 0.3 Å for distance constraints and 3° for dihedral angle constraints. These structures had good geometry and energies (data not shown) and are used strictly for illustrative purposes; quantitative comparisons between native and P-His HPr structures were based upon pairwise comparisons of the sets of structures in X-PLOR.

Acknowledgments

We thank Mark O'Neil-Johnson for acquiring the ^{1}H-^{13}C-HCCH-TOCSY and ^{1}H-^{13}C NOESY-HMQC spectra on native HPr (Brüker Instruments), Osnat Herzberg for providing coordinates for the model of the HPr–EIIA complex, Neil Jacobsen for assigning the ^{13}C resonances of native HPr, Jonathan Reizer for providing Enzyme I, Ad Bax for providing pulse sequences for the water-NOESY and -ROESY experiments, and Peter Brzovic and Carol Rohl for critical reading of this manuscript. This work was supported by NIH RO1 DK35187. We acknowledge a generous gift from the M.J. Murdock Charitable Trust for NMR instrumentation.

References

Archer SJ, Ikura M, Torchia DA, Bax A. 1991. An alternative 3D NMR technique for correlating backbone ^{15}N with side chain H_β resonances in larger proteins. *J Magn Reson 95*:636–641.

Bax A, Clore GM, Gronenborn AM. 1990. ^{1}H-^{1}H Correlation via isotropic mixing of ^{13}C magnetization, a new three-dimensional approach for assigning ^{1}H and ^{13}C spectra of ^{13}C-enriched proteins. *J Mag Reson 88*:425–431.

Bax A, Griffey RH, Hawkins BL. 1983. Correlation of proton and nitrogen-15 chemical shifts by multiple quantum NMR. *J Mag Reson 55*:301–315.

Brünger AT. 1993. *X-PLOR manual version 3.1: A system for crystallography and NMR*. Yale University Press: New Haven CT.

Delaglio F, Grzesiek S, Vuister GW, Zhu G, Pfeifer J, Bax A. 1995. NMRPipe: A multidimensional spectral processing system based on UNIX pipes. *J Biomol NMR 6*:277–293.

Farrow N, Muhandiram R, Singer AU, Pascal SM, Kay CM, Gish G, Shoelson SE, Pawson T, Forman-Kay JD, Kay LE. 1994. Backbone dynamics of a free and a phosphopeptide-complexed Src homology 2 domain studied by ^{15}N NMR relaxation. *Biochemistry 33*:5984–6003.

Ferrin TE, Huang CC, Jarvis LE, Longridge R. 1988. The MIDAS display system. *J Mol Graphics 6*:13–27.

Garrett DS, Powers R, Gronenborn AM, Clore GM. 1991. A common sense approach to peak picking in two-, three-, and four-dimensional spectra using automatic computer analysis of contour diagrams. *J Magn Reson 95*:214–220.

Grzesiek S, Bax A. 1993. Measurement of amide proton exchange rates and NOEs with water in ^{13}C/^{15}N-enriched calcineurin B. *J Biomol NMR 3*:627–638.

Herzberg O. 1992. An atomic model for the protein–protein phosphoryl group transfer. *J Biol Chem 267*:24819–24823.

Herzberg O, Klevit RE. 1994. Unraveling a bacterial hexose transport pathway. *Curr Opin Str Biol 4*:814–822.

Hol WG. 1985. The role of the alpha-helix dipole in protein function and structure. *Prog Biophys Mol Biol 45*:149–195.

Hol WG, Van Duijnen PT, Berendsen HJ. 1978. The alpha-helix dipole and the properties of proteins. *Nature 273*:443–446.

Hughes DA. 1994. Signal transduction. Histidine kinases hog the limelight. *Nature 369*:242–245.

Hurley JH, Dean AM, Thorsness PE, Hoshland DEJ, Stroud RM. 1990. Regulation of isocitrate dehydrogenase by phosphorylation involves no long-range conformational change in the free enzyme. *J Biol Chem 265*:3599–3602.

Hyberts SG, Goldberg MS, Havel TF, Wagner G. 1992. The solution structure of eglin *c* based on measurements of many NOEs and coupling constants and its comparison with X-ray structures. *Protein Sci 1*:736–751.

Ikura M, Kay LE, Tschudin R, Bax A. 1990. Three-dimensional NOESY-HMQC spectroscopy of a ^{13}C-labeled protein. *J Magn Reson 86*:204–209.

Jia Z, Quail JW, Waygood EB, Delbaere LTJ. 1993. The 2.0 Å resolution structure of *Escherichia coli* histidine-containing phosphocarrier protein HPr. *J Biol Chem 268*:22490–22501.

Johnson ML, Frasier SG. 1985. Nonlinear least-squares analysis. *Methods Enzymol 117*:301–342.

Kabsch W, Sander C. 1983. Dictionary of protein secondary structure: Pattern recognition of hydrogen-bonded and geometrical features. *Biopolymers 22*:2577–2637.

Kalbitzer HR, Hengstenberg W. 1993. The solution structure of the histidine-containing protein (HPr) from *Staphylococcus aureus* as determined by two-dimensional ^{1}H-NMR spectroscopy. *Eur J Biochem 1993*:205–214.

Kay LE, Xu GY, Singer AU, Muhandiram DR, Forman-Kay JD. 1993. A gradient-enhanced HCCH-TOCSY experiment for recording side chain ^{1}H and ^{13}C correlations in H_2O samples of proteins. *J Magn Reson B 101*:333–337.

Liao DI, Herzberg O. 1994. Refined structures of the active Ser83 → Cys and impaired Ser46 → Asp histidine-containing phosphocarrier proteins. *Structure 2*:1203–1216.

Liao DI, Silverton E, Seok YJ, Peterkofsky A, Davies DR. 1996. The first step in sugar transport: Crystal structure of the amino terminal domain of enzyme I of the *E. coli* sugar phosphotransferase system and a model of the phosphotransfer complex with HPr. *Structure 4*:861–872.

Majumdar A, Zuiderweg RP. 1993. Improved ^{13}C-resolved HSQC-NOESY spectra in H_2O, using pulsed field gradients. *J Mag Reson B 102*:242–244.

Matthews HR. 1995. Protein kinases and phosphatases that act on histidine, lysine, or arginine residues in eukaryotic proteins: A possible regulator of the mitogen-activated protein kinase cascade. *Pharmacology and Therapeutics 67*:323–350.

Nilges M, Clore GM, Gronenborn AM. 1988. Determination of the three-dimensional structure of proteins from interproton distance data by hybrid distance geometry–dynamical simulated annealing calculations. *FEBS Lett 229*:317–324.

Pelton JG, Torchia DA, Meadow ND, Roseman S. 1992. Structural comparison of phosphorylated and unphosphorylated forms of III^{glc}, a signal-transducing protein from *Escherichia coli*, using three-dimensional NMR techniques. *Biochemistry 31*:5215–5224.

Peng JW, Wagner G. 1994. Investigation of protein motions via relaxation measurements. *Methods Enzymol 239*:563–595.

Postma PW, Lengeler JW, Jacobsen GR. 1993. Phosphoenolpyruvate:carbohydrate phosphotransferase systems of bacteria. *Micro Rev 57*:543–594.

Pullen K, Rajagopal P, Branchini BR, Huffine ME, Reizer J, Saier MH Jr, Scholtz JM, Klevit RE. 1995. Phosphorylation of serine-46 in HPr, a key regulatory protein in bacteria, results in stabilization of its solution structure. *Protein Sci 4*:2478–2486.

Rajagopal P, Waygood EB, Klevit RE. 1994. Structural consequences of histidine phosphorylation: NMR characterization of the phosphohistidine from of histidine-containing protein from *Bacillus subtilis* and *Escherichia coli*. *Biochemistry 33*:15271–15282.

Reizer J, Sutrina SL, Saier MH Jr, Stewart GC, Peterkofsky A, Reddy P. 1989. Mechanistic and physiological consequences of HPr(ser) phosphorylation on the activities of the phosphoenolpyruvate:sugar phosphotransferase sys-

tem in Gram-positive bacteria: Studies with site-specific mutants of HPr. *EMBO J 8*:2111–2120.

Sklenar V, Piotto M, Leppik R, Saudek V. 1993. Gradient-tailored water suppression for ^{1}H-^{15}N HSQC experiments optimized to retain full sensitivity. *J Magn Reson A 102*:241–245.

Spera S, Ikura M, Bax A. 1991. Measurement of the exchange rates of rapidly exchanging amide protons: Application to the study of calmodulin and its complex with a myosin light chain kinase fragment. *J Biomol NMR 1*:155–165.

Swanson RV, Alex LA, Simon MI. 1994. Histidine and aspartate phosphorylation: Two-component systems and the limits of homology. *Trends Biochem Sci 19*:485–490.

Van Nuland NAJ, Boelens R, Scheek RM, Robillard GT. 1995. High-resolution structure of the phosphorylated form of the histidine-containing phosphocarrier protein HPr from *Escherichia coli* determined by restrained molecular dynamics from NMR-NOE data. *J Mol Biol 246*:180–193.

Van Nuland NAJ, Hangyi IW, Van Schaik RC, Berendsen HJC, Van Gunsteren WF, Scheek RM, Robillard GT. 1994. The high-resolution structure of the histidine-containing phosphocarrier protein HPr from *Escherichia coli* determined by restrained molecular dynamics from nuclear magnetic resonance nuclear Overhaüser effect data. *J Mol Biol 237*:544–559.

Van Nuland NAJ, Wiersma JA, Van der Spoel D, De Groot BL, Scheek RM, Robillard GT. 1996. Phosphorylation-induced torsion-angle strain in the active center of HPr, detected by NMR and restrained molecular dynamics. *Protein Sci 5*:442–446.

Wittekind MG, Klevit RE. 1991. *NMR studies of two related phosphotransfer proteins*. ESCOM: The Netherlands.

Wittekind M, Rajagopal P, Branchini BR, Reizer J, Saier MH Jr, Klevit RE. 1992. Solution structure of the phosphocarrier protein HPr from *Bacillus subtilis* by two-dimensional NMR spectroscopy. *Protein Sci 1*:1363–1376.

Wittekind M, Reizer J, Klevit RE. 1990. Sequence-specific ^{1}H NMR resonance assignments of *Bacillus subtilis* HPr: Use of spectra obtained from mutants to resolve spectral overlap. *Biochemistry 29*:7191–7200.

Worthylake D, Meadow ND, Roseman S, Liao DI, Herzberg O, Remington SJ. 1991. Three-dimensional structure of the *Escherichia coli* phosphocarrier protein III^{glc}. *Proc Natl Acad Sci USA 88*:10382–10386.

Zhang O, Kay LE, Olivier JP, Forman-Kay JD. 1994. Backbone ^{1}H and ^{15}N resonance assignments of the N-terminal SH3 domain of drk in folded and unfolded states using enhanced-sensitivity pulsed field gradient NMR techniques. *J Biomol NMR 4*:845–858.

Zheng J, Knighton DR, Ten Eyck LF, Karlsson R, Xuong N, Taylor SS, Sowadski JM. 1993. Crystal structure of the catalytic subunit of cAMP-dependent protein kinase complexed with MgATP and peptide inhibitor. *Biochemistry 32*:2154–2161.